Invited Paper

Silicon on sapphire and SOI photonic devices for mid-infrared and near-IR wavelengths

Ozdal Boyraz[*a,b], Yuewang Huang[a], Xinzhu Sang[c]
[a]EECS Department, University of California, Irvine, 92697, US
[b]EE Department at Istanbul Sehir University, Istanbul, Turkey
[c]Beijing University of Posts and Telecommunications, State Key Laboratory of Information Photonics and Optical Communications, P.O. Box 72 (BUPT), Beijing 100876, China

ABSTRACT

Conventional SOI waveguide technology, serving as the foundation of near-IR photonics, meets its limitation in mid-IR due to high loss associated with the buried oxide. Silicon-on-sapphire (SOS) waveguides are considered as a good mid-IR alternative, because the transparency window of sapphire is up to 6 μm and SOS waveguides are compatible with SOI technology. We show that properly-designed SOS waveguides can facilitate frequency band conversion between near-IR and mid-IR. An indirect mid-IR detection scheme is proposed and the mid-IR signal is down-converted to telecommunication wavelength (1.55 μm) through SOS waveguides and indirectly detected by near-IR detectors. The performance of the indirect mid-IR detection scheme is discussed. Particularly we model and compare the noise performance of the indirect detection with direct detection using state-of-the-art mid-IR detectors. In addition to advantages of room temperature and high-speed operation, the results show that the proposed indirect detection can improve the electrical signal-to-noise ratio up to 50dB, 23dB and 4dB, compared to direct detection by PbSe, HgCdTe and InSb detectors respectively. The improvement is even more pronounced in detection of weak MWIR signals. In order to further boost the performance, we also investigate mechanisms to increasing the conversion efficiency in SOS waveguide wavelength converters. The conversion efficiency can be improved by periodically cascading SOS waveguide sections with opposite dispersion characteristics to achieve quasi-phase-matching. Conversion efficiency enhancement over 30dB and the conversion bandwidth increased by 2 times are demonstrated, which may facilitate the fabrication of parametric oscillators that can improve the conversion efficiency by 50dB.

Keywords: Wavelength conversion, Waveguide, Quasi phase matching, Mid-IR detection

1. INTRODUCTION

Mid wavelength infrared (MWIR) spectral range has drawn the attention of many researchers as the window for a wide variety of applications, including free space communication, thermal and biomedical imaging, optical sensing, chemical spectroscopy and military applications as missile guidance/countermeasures[1-5]. While these applications are mostly achieved through free-space optics, their waveguided alternatives are far more attractive. In telecommunication wavelength, silicon-on-insulator (SOI) waveguide is the most widely-used platform. However, this convenience cannot be easily extended to MWIR wavelengths due to high loss associated with the SiO_2 insulator substrates in this window [6]. Among all proposed solutions, silicon-on-sapphire (SOS) waveguide is a good way to circumvent this limitation, because sapphire substrate has a transparent window all the way up to 6 μm [7]. SOS wafers are commercially available and a real instance of fabricated SOS waveguide with low loss has been

* Email: oboyraz@uci.edu

Silicon Photonics and Photonic Integrated Circuits III, edited by Laurent Vivien, Seppo K. Honkanen, Lorenzo Pavesi, Stefano Pelli, Proc. of SPIE Vol. 8431, 843104 · © 2012 SPIE · CCC code: 0277-786X/12/$18 · doi: 10.1117/12.924905

reported recently [8]. Recently, we proposed a frequency band converter based on silicon-on-sapphire (SOS) waveguide capable of converting near-IR (1.55μm) to selected band of mid-IR signals [9]. While this type of wavelength down-conversion is widely proposed to amplify mid-IR signals and generate mid-IR source [10-11], it can also be inversely utilized to solve the mid-IR light detection problem [12]. Compared to wavelength conversion in nonlinear crystals, waveguide-based wavelength converters can provide a chip-scale integrated solution with high effective nonlinearity due to its high optical confinement [11, 13]. According to the reciprocal principle, those near-IR to mid-IR converters are also capable of converting mid-IR signal in the same band to the telecommunication wavelength [14]. Here, we propose an indirect detection scheme for mid-IR signal by using near-IR detectors based on these converters. Since detectors at telecommunication wavelengths exhibit superior performances in terms of speed, noise and sensitivity, the indirect detection scheme can be a promising candidate to improve the detection performance. Meanwhile, the four-wave-mixing wavelength conversion process is an instantaneous process and the speed in indirect detection is only limited by the near-IR detectors used after the converter. This enables much faster processing of mid-IR signal than the direct detection. Also with the benefit of lower noise in near-IR detectors, the indirect scheme is possible to achieve the same signal-to-noise ratio (SNR) without any cooling. To address this point, we analyze limits of indirect detection of mid-IR signals by frequency band conversion in SOS waveguides and investigate signal-to-noise-ratio (SNR) improvement that is attainable with respect to direct detection using state of the art commercial detectors. In particular we provide a comparative investigation on the noise performance in detection of 4μm mid-IR signals by using PbSe, HgCdTe and InSb mid-IR detectors, and InGaAs photodetectors following a SOS channel waveguide based wavelength converter. We show that the proposed indirect detection can improve the electrical SNR (eSNR) up to 40dB with respect to direct detection, where the improvement is more pronounced in detection of weak incident signals.

We also work on further improving the detection performance by optimizing the wavelength conversion efficiency in the SOS waveguides. We investigate options to increase their conversion efficiency without pushing to higher pumping intensity. Up to date, several techniques have been used to enhance these figures of merits [15, 16]. However, the most widely-used quasi-phase-matching technique is only intensively investigated in periodically poled lithium niobate waveguides or optical fibers [15-17]. There is no report on quasi-phase-matching in pure silicon waveguides so far to the best of our knowledge. While particularly for large waveguides working at mid-IR wavelengths that can be fabricated by using photolithography, large geometry provides adequate manipulability for quasi-phase-matching. We conclude that this mechanism will work also on large cross-sectional SOI waveguides. The wavelength conversion efficiency based on four-wave-mixing process in silicon can be boosted by preserving the phase-matching condition through this quasi-phase-matching technique. In this report, we investigate quasi phase matching techniques that can deliver high conversion efficiencies by using large waveguide geometries that can be fabricated by using photolithography. In particular we show that alternating waveguide widths that can reset the phase mismatch in both SOI and SOS waveguides and produce wavelength conversion efficiencies >30dB larger than straight waveguides.

2. Waveguide Design and Dispersion Engineering

As we all know, the material dispersion of silicon is in the normal dispersion region for MWIR, while Sapphire has an anomalous material dispersion in this range. This implies that dispersion in SOS waveguides can be compensated between silicon and sapphire through the waveguide/substrate modal interaction [9, 18]. A flatter dispersion curve with zero dispersion wavelength (ZDWL) in MWIR is achievable and this can results in a very good condition for phase-matching in nonlinear processes, particularly four-wave-mixing (FWM) in this design. We characterize all the dispersion properties by electromagnetic simulation using a finite-element method (FEM) in COMSOL [19]. A typical dispersion curve is shown in Figure 1. The modal profile demonstrates a good confinement and the blue dispersion curve shows a very flat profile in the mid-IR range. With the flat dispersion cure, we have ZDWLs in MWIR region and these ZDWLs are tunable over a wide wavelength range. By choosing the pump wavelength slightly above ZDWL, phase-matching in FWM are possible even when signal and idler wavelengths are widely

spaced from pump wavelength. This phenomenon gives rise to a discrete band parametric nonlinear process [9]. Proper design of the waveguide geometries can meet the phase-matching condition for different signal and pump wavelengths combinations, which will result in an idler wavelength covering almost the entire mid-IR band. This provides adequate tunablity over wavelength by geometry controlling, as will be shown in upcoming sections.

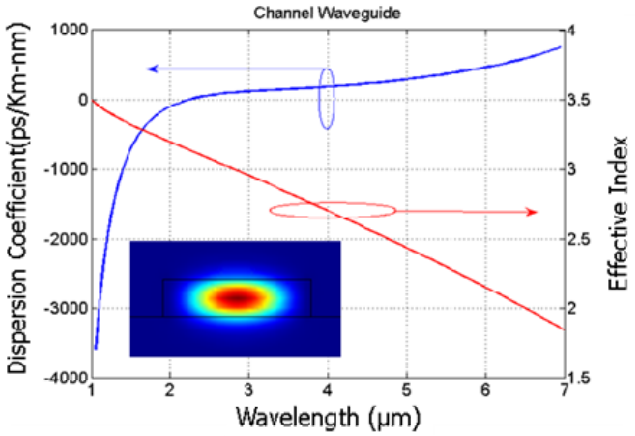

Figure 1. Dispersion of channel waveguide (blue: dispersion coefficient, red: effective index, inset: modal profile)

3. Wavelength Conversion

With the presence of the FWM process, a strong pumping power can enable the conversion of signal from one wavelength to another [14]. The energy on the pump is transferred to both the signal and idler. This parametric process is numerically characterized by solving the famous nonlinear Schrödinger Equation [14]. Conventional treatment of these differential equations is carried out under the assumption of small wavelength spacing and uniform overlap integral. In this discrete band wavelength conversion process, however, the pump, signal and idler wavelengths are spanning from near-IR to mid-IR and conventional simplified form of Schrödinger Equation is no longer valid for accurate assessment. A modified form of Schrödinger Equation as in Eq.(1) is adopted throughout the analysis. The effective areas accounting for overlap integrals between different wavelengths are independently evaluated with EM simulations. By solving these equations, we calculate the conversion efficiency defined as the output power of the idler normalized by the input signal power.

$$\begin{aligned}
\frac{dA_p}{dz} &= -\frac{\alpha_p}{2}A_p + \frac{j2\pi n_2}{\lambda_p}\left[\frac{A_p^2}{A_{eff}^{pp}} + \frac{2A_s^2}{A_{eff}^{sp}} + \frac{2A_i^2}{A_{eff}^{ip}}\right]A_p + \frac{j2\pi n_2}{\lambda_p A_{eff}^{fwm}} A_p^* A_s A_i e^{j\Delta kz} \\
\frac{dA_s}{dz} &= -\frac{\alpha_s}{2}A_s + \frac{j2\pi n_2}{\lambda_s}\left[\frac{A_s^2}{A_{eff}^{ss}} + \frac{2A_p^2}{A_{eff}^{ps}} + \frac{2A_i^2}{A_{eff}^{is}}\right]A_s + \frac{j2\pi n_2}{\lambda_s A_{eff}^{fwm}} A_p A_p A_i^* e^{-j\Delta kz} \\
\frac{dA_i}{dz} &= -\frac{\alpha_i}{2}A_i + \frac{j2\pi n_2}{\lambda_i}\left[\frac{A_i^2}{A_{eff}^{ii}} + \frac{2A_p^2}{A_{eff}^{pi}} + \frac{2A_s^2}{A_{eff}^{si}}\right]A_i + \frac{j2\pi n_2}{\lambda_i A_{eff}^{fwm}} A_p A_p A_s^* e^{-j\Delta kz}
\end{aligned} \tag{1}$$

Figure 2(a) shows a typical wavelength conversion efficiency spectrum in SOS waveguide. Besides the conventional conversion band around the pumping wavelength, strong conversion also occurs in the sideband as a discrete conversion band [9]. This type of conversion is extremely useful to achieve wide-range wavelength conversion spanning from near-IR to mid-IR. Figure 2(b) shows that signal at 1.55um can be converted to a wide range of different mid-IR wavelengths using SOS waveguides with different geometries. This corresponds to almost the

whole mid-IR spectra and suits to a wide range of applications. The dark region in the figure corresponds to the pump wavelength region to enable the conversion from the peaked mid-IR to telecommunication wavelength. Thulium-doped fiber lasers and Chromium-based solid-state lasers can provide adequate pumping in this region [20]. Meanwhile, two-photon-absorption (TPA) and the free-carrier-absorption in the region is not pronounced, which enables high power pumping. We also investigate the dependence of conversion efficiency and peak idler wavelength over pump intensity. As shown in Figure 3, conversion efficiency saturates at high pumping levels and peak signal wavelength can be tuned by increasing pump intensity [9, 14].

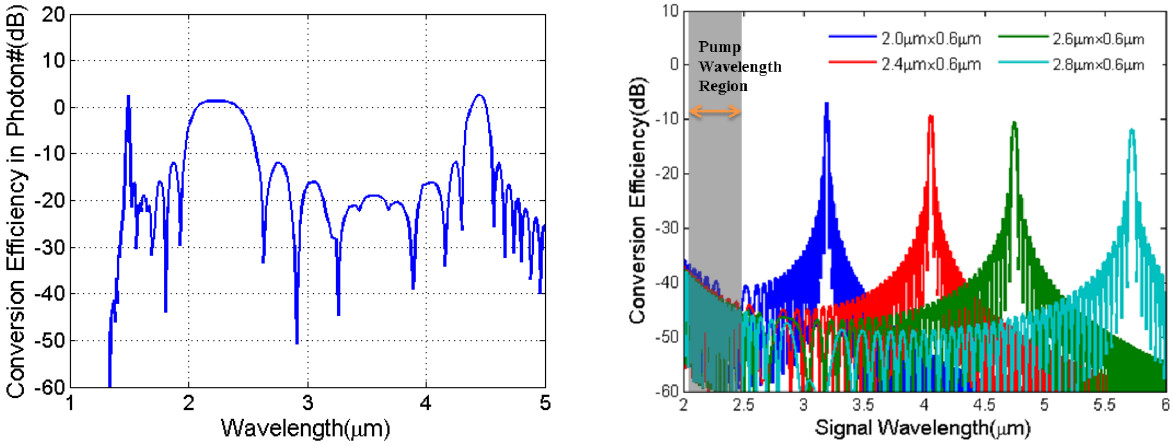

Figure.2 (a) Wavelength conversion over the entire band and strong conversion present both around the pump wavelength and in the sidebands. (b) Conversion efficiency from mid-IR to telecommunication wavelength.. The dark region in the figure corresponds to the pump wave-length region to enable the conversion from the peaked mid-IR to telecommunication wavelength. The pump wavelength is greater than the 2.2 um two-photon-absorption (TPA) upper limit.

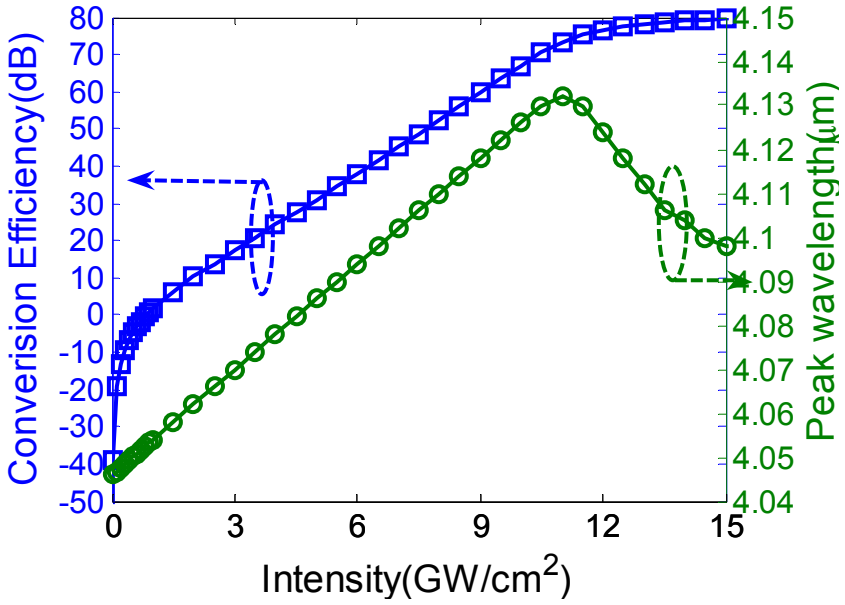

Figure 3. Conversion efficiency (blue) and peak wavelength (green) dependence on pump intensity.

4. Indirect Detection of mid-IR Signals

As stated in previous sections, the designed SOS waveguides are capable of converting mid-IR signal to telecommunication wavelength. Since near-IR detectors shows superior performance to their mid-IR alternatives, detection of mid-IR signals by indirectly detecting their near-IR replicas has the potential to improve detection performance. Figure 4 illustrates the proposed detection scheme. The upper branch illustrates the indirect detection of mid-IR signals up-converted to near-IR wavelengths and detected by telecommunication detectors (InGaAs p-i-n detectors most widely used). Here the wavelength conversion is generated through FWM based modulational instability at SOS waveguides. This wavelength conversion process is characterized in Section 3. Since detectors at telecommunication wavelengths exhibit superior performances in terms of speed, noise and sensitivity, the indirect detection scheme can be a promising candidate to improve the detection performance. Meanwhile, the four-wave-mixing wavelength conversion process is an instantaneous process and the speed in indirect detection is only limited by the near-IR detectors used after the converter. This enables much faster processing of mid-IR signal than direct detection. Also with the benefit of lower noise in near-IR detectors, the indirect scheme is possible to achieve the same signal-to-noise ratio (SNR) without any cooling.

In the next section, we will model major noise present in the indirect detection and comparatively in direct detection. Based on this, we analyze limits of indirect detection of mid-IR signals by frequency band conversion in SOS waveguides and investigate signal-to-noise-ratio (SNR) improvement that is attainable with respect to direct detection using state of the art commercial detectors. In particular we provide a comparative study on the noise performance in detection of 4μm mid-IR signals by using PbSe, HgCdTe and InSb mid-IR detectors, and InGaAs photodetectors following a SOS channel waveguide based wavelength converter.

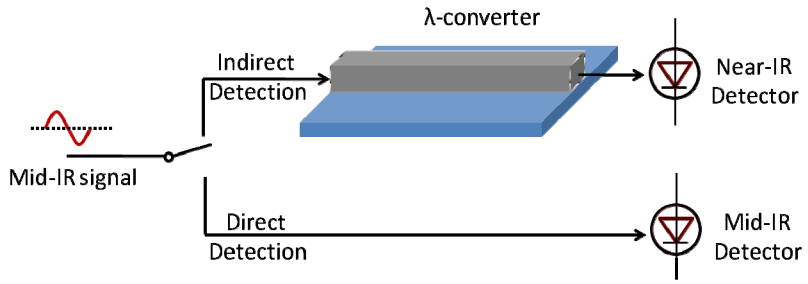

Figure 4. Schematics of direct and indirect mid-IR detection.

5. Noise Modeling

Noise in indirect detection may originate from wavelength conversion process or the detector itself. Noise associated with wavelength conversion includes quantum noise, Raman induced noise and pump transferred noise. Since the frequency separation is more than three times wider than the Raman shift in silicon the Raman induced noise is negligible. Also, the noise transfer from pump is considered to be detrimental for large signal powers, pump lasers with RIN>120dB/Hz and large phase noise [21-22]. Since the noise performance of mid-IR pump lasers is not well characterized, we intentionally exclude the noise originating from the pump lasers in our calculations. However, excess quantum noise is always present in the parametric process and will be transferred to InGaAs-based p-i-n detector as quantum fluctuations, $i_{n,qt}^2$, described as [23]:

$$i_{n,qt}^2 = 4R^2 G_i P_{in} \frac{h\nu}{2}(2G_i + 1)B_e \qquad (2)$$

Here, R is the responsivity of the detector, B_e is the electrical bandwidth, P_{in} is the incident power and G_i is the conversion efficiency numerically calculated by solving nonlinear Schrödinger Equation in SOS waveguide as shown in Figure 2(a). Other detector noise components in the InGaAs detector include thermal noise $i_{n,th}^2$ and shot noise $i_{n,sh}^2$ as in Equation(3) and (4), in which R_L is load resistance, F_n is the circuitry noise figure [24].

$$i_{n,th}^2 = 4\left(k_b T / R_L\right) F_n B_e \qquad (3)$$

$$i_{n,sh}^2 = 2q\left(RP_{in} + i_d\right)B_e \quad (4)$$

Lower arm in Figure 1 illustrates the direct detection of mid-IR signals. Commercial mid-IR detectors include photoconductive, photovoltaic and thermal detectors. Thermal detectors are too slow for real-time application, and hence only photoconductive and photovoltaic detectors are analyzed here. Photovoltaic detectors absorb photons with energy beyond and near their bandgap to generate current. Because the energy associated with mid-IR photons corresponds to a narrow bandgap, thermal generation can result in considerable dark current. Low temperature operation is always necessary to suppress dark current and the shot noise associated with it. The noise components in photovoltaic detectors include thermal noise, shot noise and flicker noise. If a low-pass filter is inserted to eliminate flicker noise, the total noise $i_{n,pv}^2$ will mainly consist of thermal noise $i_{n,th}^2$ and shot noise $i_{n,sh}^2$ as in Equation (3) and (4).

In photoconductive mode, photo-generated carriers change the conductivity of the medium and lead to a change on the voltage across the medium. Due to different detection mechanism, the noise composition in photoconductive detectors is also different from photovoltaic ones. Main noise components in photoconductive detectors include thermal noise, generation-recombination noise (GR-noise), background noise, flicker noise and also the noise transferred from voltage supply. While supply voltage induced noise can be minimized to negligible level by using low noise voltage supplies and flicker noise can also be eliminated by low-pass filters, the total noise $i_{n,pc}^2$ mainly includes thermal noise $i_{n,th}^2$, GR-noise $i_{n,gr}^2$ and background noise $i_{n,bg}^2$ [25-26]:

$$i_{n,gr}^2 = \int_0^{B_e} \frac{4qI_0\Gamma_G}{(1+4\pi^2 f^2\tau^2)}df = \frac{2qI_0\Gamma_G}{\pi\tau}\tan^{-1}(2\pi B_e\tau) \quad (5)$$

$$i_{n,bg}^2 = q^2\eta A E_{BB} B_e \quad (6)$$

Where τ is average carrier lifetime, I_0 is the total generation current, Γ_G is the current gain, η is quantum efficiency, A is active detector area, $E_{BB} = \int_0^{\lambda_c} \varepsilon_\lambda \frac{2\pi c}{\lambda^4}\left[\frac{1}{e^{hc/\lambda k_b T} - 1}\right]d\lambda$ is the total photon flux density with λ_c being the cut-off wavelength and ε_λ the emissivity for the window material.

6. Noise performance and eSNR improvement

To assess the detection limit and evaluate noise performance we used state-of-the-art commercial mid-IR and near-IR photo-detectors in our calculation. In particular, we use InGaAs PIN detector for near-IR detection in indirect scheme. For direct mid-IR detection, three types of detectors are widely used: InSb photovoltaic, PbSe photoconductive HgCdTe photoconductive detector. While PbSe and HgCdTe detectors can work properly at room temperature, InSb detectors usually require liquid-nitrogen or multi-stage TE cooling. Their main parameters of these used detectors are listed in Table 1, which tracks the up-to-date commercial detectors, e.g. Hamamatsu and Vigo [27, 28]. An electrical bandwidth of 0.1MHz is used to accommodate the relatively slow mid-IR detectors. Figure 4 illustrates the noise at InGaAs detector after the wavelength-converter at room temperature with incident power level of 1μW. At low pump intensities, the detection system will be limited by shot noise. As pump intensity increases above 0.4GW/cm^2, the conversion efficiency increases and the quantum noise becomes dominant. Thermal noise is minor and cooling of near-IR detector cannot further improve the noise performance in indirect detection.

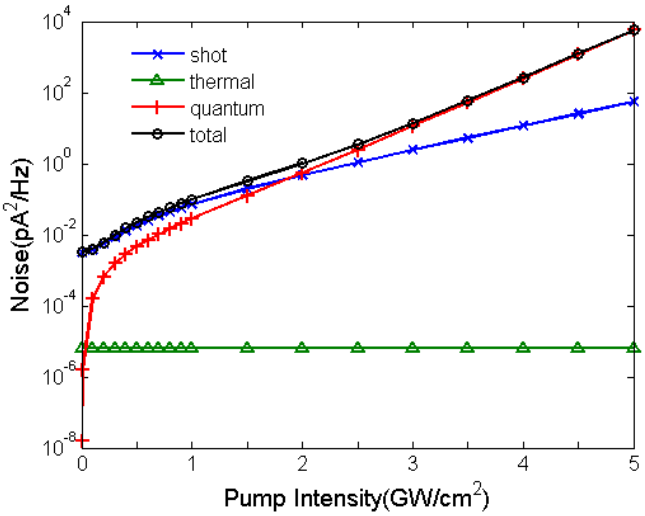

Figure 5. Detection noises at near-IR InGaAs detector in indirect detection

Table 1. Detector parameters

	T(K)	λ_{op}(μm)	R	$R_L(\Omega)$	I_d	NEP(W/Hz$^{1/2}$)
InGaAs	300	1.55	0.95[A/W]	8M	80pA	2×10^{-15}
PbSe	300	4.0	3×10^{3}[V/W]	0.3M	N/A	8×10^{-11}
HgCdTe	293	4.0	3×10^{3}[V/W]	1K	N/A	3.1×10^{-12}
InSb	77	4.0	2.5[A/W]	1M	10μA	5.5×10^{-13}

For direct detection at mid-IR, thermal noise dominates in PbSe and HgCdTe detectors and shot noise is the dominant noise in the liquid nitrogen cooled InSb detectors. We estimate that for the same 1μW input power level at mid-IR the total noise current in PbSe, HgCdTe and InSb detectors to be $0.10\,pA/\sqrt{Hz}$, $4.09\,pA/\sqrt{Hz}$ and $1.63\,pA/\sqrt{Hz}$ respectively.

Electrical Signal to Noise Ratio (eSNR) is often used as performance metric. To assess the noise improvement through indirect detection we estimate the eSNR of detectors at three different incident power levels of 0.1 μW, 1 μW and 10 μW which are measured at the input of mid-IR detectors and at the input of the SOS wavelength converter. The eSNR enhancement is evaluated by comparing the eSNR results of three mid-IR detectors to that of the InGaAs detector as: $eSNR_{near-IR}/eSNR_{mid-IR}$, as illustrated in Figure 6(a). At an incident power level of 1μW, liquid nitrogen cooled InSb detectors can achieve about the same eSNR as indirect detection at 1550nm. However, indirect detection can provide >10 dB, and >35dB eSNR improvement over direct detection using HgCdTe and PbSe detectors, respectively. The eSNR improvement in these detectors is achieved for pump intensities above 0.1GW/cm^2 at which conversion efficiency exceeds -20dB. At the pump intensities below 1 GW/cm^2, the indirect detection will be limited by thermal and shot noised and we obtain increasing eSNR with increasing conversion efficiency. However, at pump intensities above 1GW/cm^2 the indirect detection will be limited by the quantum noise of the parametric process and the eSNR improvement will saturate at 40dB level with respect to PbSe detector for 1μW input power. The advantage of indirect detection will be more obvious for low input power levels. For instance, the SNR improvement with respect to PbSe can go up to 50 dB for 0.1μW input power levels. Moreover, we even expect that indirect detection can provide 7dB eSNR improvement with respect to liquid nitrogen cooled InSb detectors at such low power levels.

The eSNR improvement is wavelength dependent as the conversion efficiency for fixed pump intensity. As Figure 6(b) illustrates, we can attain eSNR improvements within up to 300nm, 200nm conversion bandwidths centered at 4μm for input power levels of 0.1μW with respect to PbSe and InSb detectors, respectively. Although the quantum

noise saturates the eSNR improvement at the peak conversion wavelength, eSNR improvement bandwidth increases with increasing pump intensity. This is consistent with the tendency on conversion bandwidth increase with increasing pump intensity [29].

As indicated in Figure 6(a), the eSNR improvement saturates at high pump intensities. This is due to the fact that output signal power and noise power relate with conversion efficiency with the same polynomial order dependence when quantum noise becomes dominant at high pump intensity level. However, this does not means there is no benefit on playing with the pump intensity. At this point, we also investigate the possibility of achieving the same conversion efficiency level with lower pump intensities. In our case, the conversion efficiency is boosted by using quasi-phase-matching in SOS and SOI waveguides, as will be shown in next section.

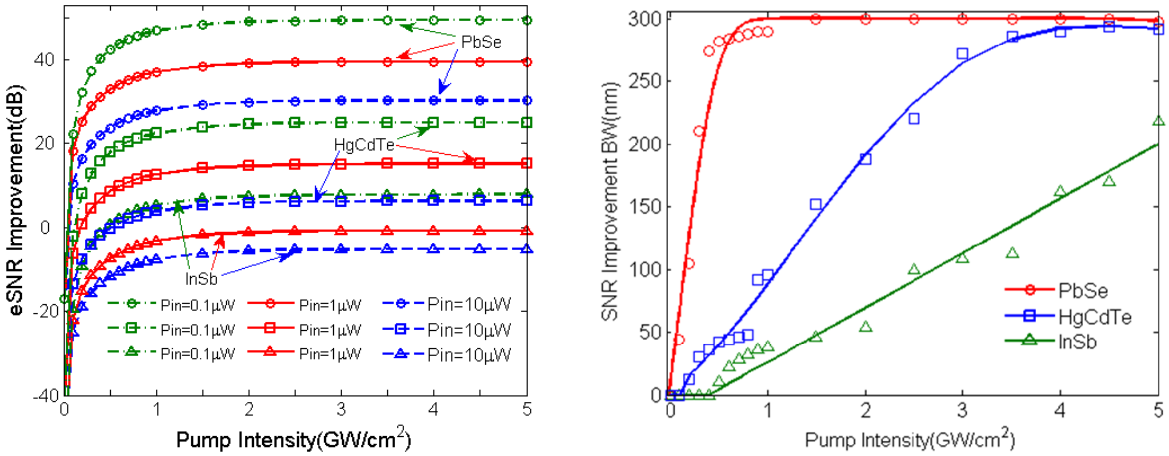

Figure 6. (a) eSNR improvement by using indirect detection with respect to direct detection. PbSe and HgCdTe photoconductive detector is set to operate at room temperature and InSb photovoltaic detector is liquid nitrogen cooled to 77K. (b) Bandwidth on which there is SNR improvement by using indirect detection increase almost linearly with intensity after the threshold and before saturation (Pin=0.1μW).

7. Conversion Efficiency Improvement using Quasi Phase Matching

With low phase-mismatch, energy is transferred from pump to signal and idler. However, when phase-mismatch is larger than π, the energy will be transferred back in the opposite way. If we cascade sections with opposite dispersion coefficient at specific wavelength, phase-mismatch will be compensated and the energy will be constantly transferred to idler, which can enhance the conversion efficiency. Figure 7 illustrates the concept of quasi-phase-matching in silicon waveguides and the alternating sections are channel waveguides with different widths but the same height. The fabrication of alternating sections with large geometries is feasible. Figure 8(a) shows that the idler power increases continuously along the SOI waveguide if we repeatedly compensate the phase to preserve a positive phase-mismatch for FWM. Figure 8(b) is the corresponding conversion efficiency spectrum. The two alternating sections are 2.4μm×0.6μm and 2.8μm×0.6μm respectively. The conversion efficiencies without quasi-phase-matching with the same total waveguide length for the two straight waveguides are -17.0dB and -23.8dB, which means that the conversion efficiency is enhanced by more than 30dB with quasi phase matching. Figure 8(c) and (d) are similar results in SOS waveguides as (a) and (b). The two alternating sections are 2.3μm×0.6μm and 2.8μm×0.6μm. With 3cm uniform waveguides of 2.3μm ×0.6μm and 2.8μm×0.6μm given conversion efficiency of -4.0dB and -22.3dB respectively in SOS waveguide, >30dB enhancement is also achievable.

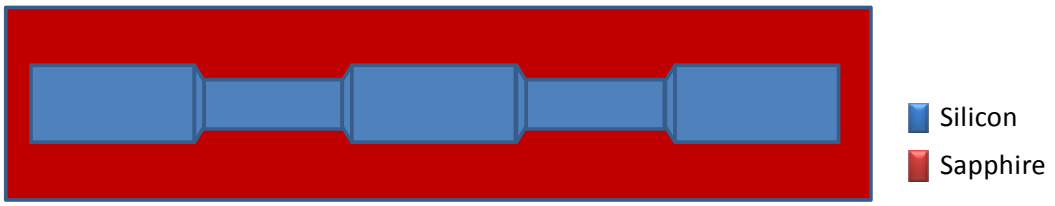

Figure 7. A conceptual illustration of quasi phase matching in SOS waveguide, waveguides are channel waveguide with no height variation.

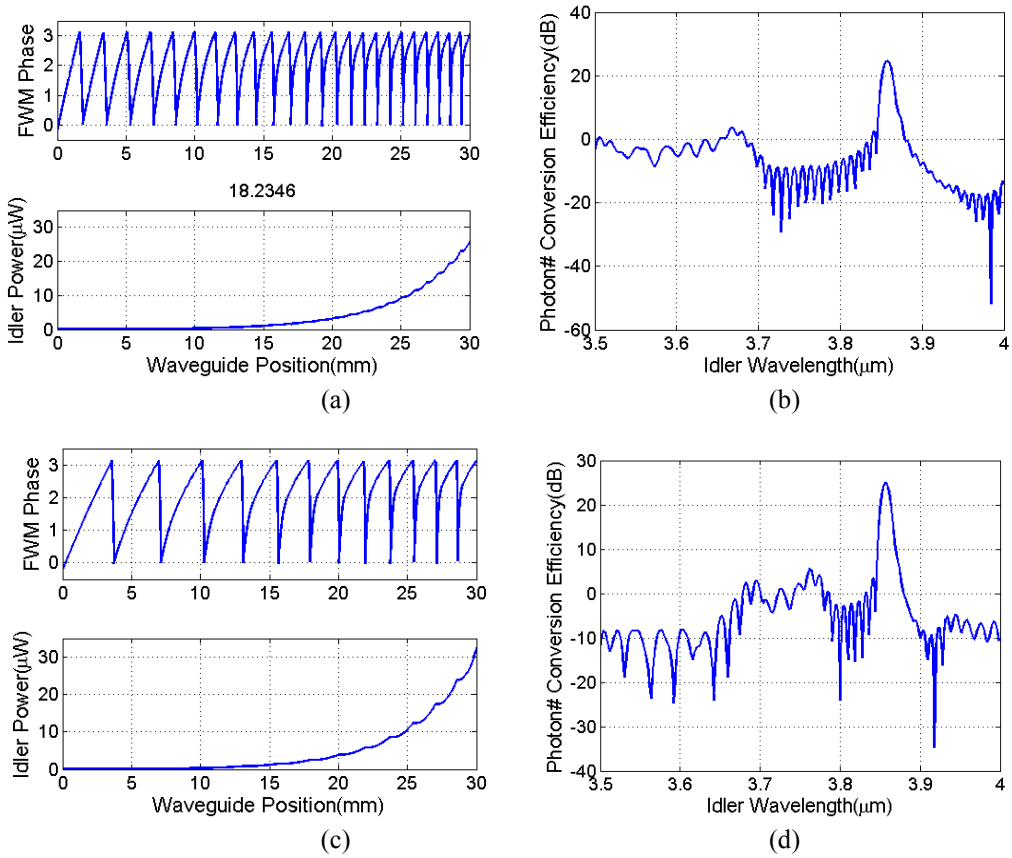

Figure 8. Conversion Efficiency enhancement by QFM.

In a similar fashion, if we cascade sections with opposite dispersion slope yet the same overlapped ZDWL, phase-mismatch can be compensated both below and above ZDWL. Efficient conversion is possible over a broader bandwidth. Conversion bandwidth can be enhanced by this quasi-phase-matching (QFM) mechanism. Figure 9 shows the effects of QFM on bandwidth enhancement. Blue and green curve are spectrum for uniform waveguide structures and the red curve is the conversion efficiency spectrum when the two sections are periodically cascaded. Bandwidth is broadened by about a factor of 2.

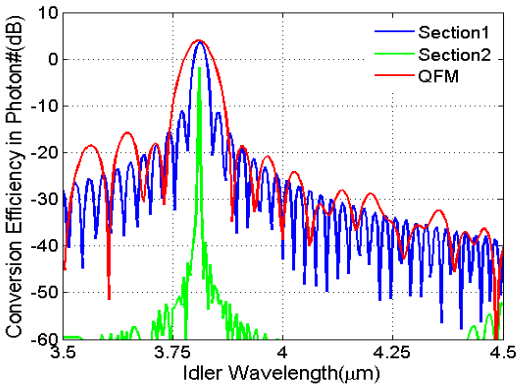

Figure 9 Conversion bandwidth enhancement by QFM.

8. OPO design

In order for more practical conversion and lasing, an optical cavity is formed to support optical parametric oscillation [30]. Here we designed a linear cavity for demonstrating purpose. Because the spacing between signal, pump and idler are large, it is easy to design cavity mirrors selectively reflect the idler wavelength. This makes a cavity for idler only and makes it easier to manipulate pulse operation. The cavity is 7.25mm long and this reduces the walk-off between pump and signal and hence alleviates the idler pulse spreading. Figure 10 shows the wavelength conversion efficiency in the designed OPO. A conversion efficiency of >40dB is achieved with a pumping intensity of 5W/μm^2, which is 20dB more than that in a 30mm long single-pass waveguide. Also due to the oscillating effect, the bandwidth is reduced.

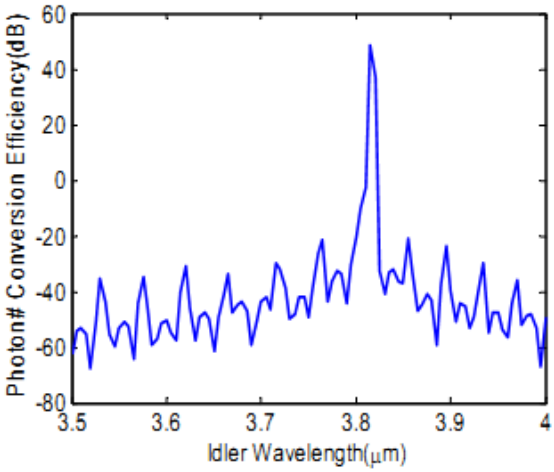

Figure 10. Conversion efficiency in optical cavity.

9. SUMMERY

Due to substrate loss, conventional SOI platforms cannot support MWIR photonic IC and planar devices on silicon-on-sapphire (SOS) are emerging as a prospective replacement. Properly-designed SOS waveguides are capable of converting selected MWIR band to SWIR, where the signals are detected with mature telecommunication detectors. We compare the noise performance of this indirect detection with direct detection using MWIR detectors and show

that, in addition to room temperature and high speed operation, the proposed indirect detection can improve the electrical signal-to-noise ratio up to 50dB, 23dB and 4dB compared to direct detection using PbSe, HgCdTe and InSb detectors respectively. The improvement is even more pronounced when the incident power is of low level. In addition, we also investigate the option to further boost the detection performance by increasing the conversion efficiency without tuning up the pumping level. The quasi-phase-matching technique is used to serve this purpose. We show that quasi phase matched SOS waveguides can provide over 30dB higher conversion efficiency and 2× more bandwidth than that can be achieved in uniform waveguide geometries. Finally by forming a cavity for the idler, the efficiency is further improved by 20dB to > 40dB.

Acknowledgement

This work is supported by DARPA Young Faculty Award (Grant No. N66001-10-1-4036) and the National Key Basic Research Special Foundation (2010CB327601).

REFERENCES

[1] Martini, R.; Bethea, C.; Capasso, F.; Gmachl, C.; Paiella, R.; Whittaker, E.A.; Hwang, H.Y.; Sivco, D.L.; Baillargeon, J.N.; Cho, A.Y.; , "Free-space optical transmission of multimedia satellite data streams using mid-infrared quantum cascade lasers," Electronics Letters , vol.38, no.4, pp.181-183, 14 Feb 2002

[2] Yury A. Bakhirkin, Anatoliy A. Kosterev, Chad Roller, Robert F. Curl, and Frank K. Tittel, "Mid-Infrared Quantum Cascade Laser Based Off-Axis Integrated Cavity Output Spectroscopy for Biogenic Nitric Oxide Detection," Appl. Opt. 43, 2257-2266 (2004)

[3] Worrell, C.A.; Giles, I.P.; Adatia, N.A.; , "Remote gas sensing with mid-infra-red hollow waveguide," Electronics Letters , vol.28, no.7, pp.615-617, 26 March 1992

[4] Albert Schliesser, Markus Brehm, Fritz Keilmann, and Daniel van der Weide, "Frequency-comb infrared spectrometer for rapid, remote chemical sensing," Opt. Express 13, 9029-9038 (2005) http://www.opticsinfobase.org/abstract.cfm?URI=oe-13-22-9029

[5]D. H. Titterton, Development of Infrared Countermeasure Technology and Systems Mid-infrared Semiconductor Optoelectronics, Springer Series in Optical Sciences, 2006, Volume 118/2006, 635-671, DOI: 10.1007/1-84628-209-8_20.

[6] Paul Klocek, "Handbook of Infrared Optical Materials", M. Dekker, New York(1991)

[7] R.A. Soref, S.J. Emelett, and W.R. Buchwald, “Silicon waveguided components for the long-wave infrared region,” Journal of Optics A: Pure and Applied Optics, vol. 8, 2006, pp. 840-848.

[8] T. Baehr-Jones, A. Spott, R. Ilic, A. Spott, B. Penkov, W. Asher, and M. Hochberg, “Silicon-on-sapphire integrated waveguides for the mid-infrared,” Optics Express, vol. 18, Jun. 2010, pp. 12127-12135.

[9] E-K Tien, Y. Huang, S. Gao, Q. Song, F. Qian, S. K. Kalyoncu, and O. Boyraz, “Discrete parametric band conversion in silicon for mid-infrared applications,” Opt. Express 18, 21981-21989 (2010).

[10] N. K. Hon, K. K. Tsia, D. R. Solli, and B. Jalali, “Periodically poled silicon,” Appl. Phys. Lett. 94, 091116 (2009)

[11] X. Liu, R.M. Osgood, Y.A. Vlasov, M. J. GreenWilliam, “Mid-infrared optical parametric amplifier using silicon nanophotonic waveguides”, Nat Photon 4, 557-560 (2010).

[12] K. Karstad, A. Stefanov, M. Wegmuller, H. Zbinden, N. Gisin, T. Aellen, M. Beck and J. Faist, Optics and Lasers in Engineering, 43, 537-544.

[13] S.Zlatanovic, J.S. Park, S.Moro, J.M. Chavez Boggio, I.B. Divliansky, N.Alic, S.Mookherjea, S.Radic, “Mid-infrared wavelength conversion in silicon waveguides using ultracompact telecom-band-derived pump source”, Nat Photon 4, 561-564 (2010).

[14] G. Agrawal, Nonlinear Fiber Optics, Fourth Edition (Academic Press, 2006)

[15] L.E. Myers, R.C. Eckardt, M.M. Fejer, R.L. Byer, W.R. Bosenberg, and J.W. Pierce, "Quasi-phase-matched optical parametric oscillators in bulk periodically poled LiNbO3," Journal of the Optical Society of America B, vol. 12, Nov. 1995, pp. 2102-2116.
[16] Jaeyoun Kim, O. Boyraz, J. Lim, and M. Islam, "Gain enhancement in cascaded fiber parametric amplifier with quasi-phase matching: theory and experiment," Lightwave Technology, Journal of, vol. 19, 2001, pp. 247-251.
[17] Yeung Lak Lee, Bong-Ahn Yu, Changsoo Jung, Young-Chul Noh, Jongmin Lee, and Do-Kyeong Ko, "All-optical wavelength conversion and tuning by the cascaded sum- and difference frequency generation (cSFG/DFG) in a temperature gradient controlled Ti:PPLN channel waveguide," Opt. Express 13, 2988-2993 (2005).
[18] M. N. Islam, and O. Boyraz, IEEE Journal of Selected Topics in Quantum Electronics, 8, 3, 527-537(2002).
[19] COMSOL Multiphysics; COMSOL, Inc., Burlington, MA (www. comsol.com/).
[20] R. Paschotta, Encyclopedia of Laser Physics and Technology (Wiley, Weinheim, Germany,2008)
[21] P. Kylemark, P. O. Hedekvist, H. Sunnerud, M. Karlsson, and P. A. Andrekson, "Noise Characteristics of Fiber Optical Parametric Amplifiers," J. Lightwave Technol. 22, 409- (2004).
[22] S. Moro, A. Peric, N. Alic, B. Stossel, and S. Radic, ""Phase noise in fiber-optic parametric amplifiers and converters and its impact on sensing and communication systems,"", Opt. Express 18, 21449-21460 (2010)
[23] P. Kylemark, P. O. Hedekvist, H. Sunnerud, M. Karlsson, and P. A. Andrekson, "Noise Characteristics of Fiber Optical Parametric Amplifiers," J. Lightwave Technol. 22, 409- (2004).
[24] G.P. Agrawal, Fiber-Optic Communication Systems, Third Edition (Wiley-Interscience 2002).
[25] S. Nudelman, "The Detectivity of Infrared Photodetectors," Appl. Opt. 1, 627-636 (1962).
[26] P. Bhattacharya, Semiconductor Optoelectronic Devices (Prentice Hall, Englewood Cliffs, NJ, 1994)
[27] Characteristics and Use of Infrared Detectors (Solid State division, Hamamatsu Photonics K.K, Tokyo, Japan, 2004).
[28] IR Detectors Catalogue (Vigo System, Ozarow Mazowiecki, Poland, 2006).
[29] R. H. Stolen and J. E. Bjorkholm, IEEE J. Quantum Electron. QE-18, 1062 (1982)
[30] R. W. Boyd, [Nonlinear optics], Academic Press(2003